polymers

MDPI

Article

Dielectric Trapping of Biopolymers Translocating through Insulating Membranes

Sahin Buyukdagli [1,*], Jalal Sarabadani [2,4] and Tapio Ala-Nissila [3,4]

1 Department of Physics, Bilkent University, Ankara 06800, Turkey
2 School of Nano Science, Institute for Research in Fundamental Sciences (IPM), Tehran 19395-5531, Iran; jalal@ipm.ir
3 Interdisciplinary Centre for Mathematical Modelling and Department of Mathematical Sciences, Loughborough University, Loughborough, Leicestershire LE11 3TU, UK
4 Department of Applied Physics and QTF Center of Excellence, Aalto University School of Science, P.O. Box 11000, FI-00076 Aalto, Espoo, Finland; Tapio.Ala-Nissila@aalto.fi
* Correspondence: buyukdagli@fen.bilkent.edu.tr; Tel.: +90-312-290-2673

Received: 15 October 2018; Accepted: 6 November 2018; Published: 9 November 2018

Abstract: Sensitive sequencing of biopolymers by nanopore-based translocation techniques requires an extension of the time spent by the molecule in the pore. We develop an electrostatic theory of polymer translocation to show that the translocation time can be extended via the dielectric trapping of the polymer. In dilute salt conditions, the dielectric contrast between the low permittivity membrane and large permittivity solvent gives rise to attractive interactions between the *cis* and *trans* portions of the polymer. This self-attraction acts as a dielectric trap that can enhance the translocation time by orders of magnitude. We also find that electrostatic interactions result in the piecewise scaling of the translocation time τ with the polymer length L. In the short polymer regime $L \lesssim 10$ nm where the external drift force dominates electrostatic polymer interactions, the translocation is characterized by the drift behavior $\tau \sim L^2$. In the intermediate length regime 10 nm $\lesssim L \lesssim \kappa_b^{-1}$ where κ_b is the Debye–Hückel screening parameter, the dielectric trap takes over the drift force. As a result, increasing polymer length leads to quasi-exponential growth of the translocation time. Finally, in the regime of long polymers $L \gtrsim \kappa_b^{-1}$ where salt screening leads to the saturation of the dielectric trap, the translocation time grows linearly as $\tau \sim L$. This strong departure from the drift behavior highlights the essential role played by electrostatic interactions in polymer translocation.

Keywords: polymer translocation; dielectric membranes; electrostatic interactions; charge screening

1. Introduction

The continuous improvement of our control over nanoscale physics allows an increasingly broader range of nanotechnological applications for bioanalytical purposes. Along these lines, the electrophoretic transport of biopolymers through nanopores can provide a surprisingly simple and fast approach for biopolymer sequencing [1–7]. This sequencing technique consists of mapping the nucleic acid structure of the translocating polymer from the ionic current signal caused by the molecule. At present, the translocation times provided by experiments are not sufficiently long for sensitive reading of this ionic current signal [6]. Thus, the technical challenge consists of reducing the polymer translocation speed by orders of magnitude from the current experimental values. Over the past two decades, this objective has motivated intensive research work with the aim to characterize the effect of various system characteristics on the polymer translocation dynamics.

Polymer translocation is driven by the entangled effects of electrostatic polymer–membrane interactions, the electrohydrodynamic forces associated with the electrophoretic and electroosmotic drags, and entropic barriers originating from conformational polymer fluctuations and hard-core

polymer–membrane interactions. Due to the resulting complexity of the translocation process, polymer translocation models have initially separately considered the contribution from electrohydrodynamic and entropic effects. Within Langevin dynamics, theoretical studies of polymer translocation first focused on the role played by entropy [8–12] (see also Refs. [13,14] for an extended review of the literature). The contribution from electrostatics and hydrodynamics on the polymer translocation dynamics has been investigated by mean-field (MF) electrostatic theories [15–18]. Within a consistent electrohydrodynamic formulation, we have recently extended these translocation models by including beyond-MF charge correlations and direct electrostatic polymer–membrane interactions [19–21].

In the theoretical modeling of polymer translocation, the current technical challenge consists of incorporating on an equal footing conformational polymer fluctuations and electrostatic effects. The achievement of this difficult task would allow for unifying the entropic coarse-grained models and electrohydrodynamic theories mentioned above. At this point, it should be noted that such a unification necessitates the inclusion of polymer–membrane interactions outside the pore, while the translocation models of Refs. [19–21] developed for short polymers and long pores included exclusively the electrostatic polymer–membrane interactions inside the pore medium. In this work, we make the first attempt to overcome this limitation and develop a non-equilibrium theory of polymer translocation explicitly including the interactions between a charged dielectric membrane and an anionic polymer of arbitrary length. Within this theory, we characterize the effect of salt and membrane charge configurations, and the polymer length on the translocation dynamics of the molecule.

In Section 2, we introduce first the geometry and charge composition of the translocation model. Then, we derive the electrostatically augmented Fokker–Planck (FP) equation characterizing the translocation dynamics, and obtain the capture velocity and translocation time. Section 3.2 considers the effect of surface polarization forces on polymer translocation through neutral membranes. Therein, we identify a *dielectric trapping* mechanism enabling the extension of the translocation time by orders of magnitude. In Section 3.3, we investigate the effect of the fixed membrane charges on the dielectric trapping and reveal an *electrostatic trapping* mechanism occuring at positively charged membranes in contact with physiological salt concentrations. We also scrutinize in detail the effect of dielectric and electrostatic interactions on the scaling of the polymer translocation time with the polymer length. Our results are summarized in the Discussion part where the limitations of our model and future extensions are discussed.

2. Materials and Methods

2.1. Charge Composition of the System

The charge composition of the system is depicted in Figure 1. The membrane of thickness d, surface charge σ_{m} of arbitrary sign, and dielectric permittivity ε_{m} are immersed in the monovalent electrolyte NaCl of concentration ρ_{b} and dielectric permittivity $\varepsilon_{\mathrm{w}} = 80$. We note in passing that, in our article, the dielectric permittivities are expressed in units of the vacuum permittivity ε_0. Moreover, the membrane contains a pore oriented along the z-axis. The externally applied voltage between the *cis* and *trans* sides of the membrane induces a uniform electric field in the pore. This field exerts a constant force f_0 on the polymer portion enclosed by the nanopore. We note that the detailed formulation of the pore electrohydrodynamics would be necessary to relate quantitatively the force f_0 to the external electric field, the polymer charge, the ion density, and the electroosmotic flow. As this task is beyond the scope of the present work, the pore electrohydrodynamics will be coarse-grained and the drift effect on the polymer translocation will be described solely in terms of the driving force f_0.

The polymer is modeled as a charged line of total length L, mass M, and the bare linear charge density of dsDNA molecules $-\lambda_{\mathrm{c}} q$ with $\lambda_{\mathrm{c}} = 2.0/(3.4\ \text{Å})$ and the electron charge $q = 1.6 \times 10^{-19}$ C. Electrostatic polymer–membrane interactions induce an additional electrostatic force on the polymer charges. Appendix D explains the derivation of the corresponding electrostatic potential from the

Debye–Hückel (DH) level electrostatic polymer grand potential. The latter is obtained by expanding the grand potential of the whole system at the quadratic order in the polymer charge [22]. In order to improve this approximation, we will make use of the variational *charge renormalization* technique [23] and evaluate the electrostatic polymer–membrane interactions in terms of the effective polymer charge density $\tilde{\lambda}_c$ defined as

$$\tilde{\lambda}_c = n\lambda_c. \tag{1}$$

The effective charge density (1) corresponds to the bare charge density λ_c dressed by the counterion cloud around the polyelectrolyte. In Equation (1), n is the charge renormalization factor whose variational evaluation is explained in Appendix A. We finally note that, in the limit of vanishing salt $\rho_b \to 0$, the charge renormalization factor tends to its *Manning limit* $n = 1/(\ell_B\lambda_c)$ [23] and the effective polymer charge (1) becomes

$$\tilde{\lambda}_c = \frac{1}{\ell_B}, \tag{2}$$

where we used the Bjerrum length $\ell_B = q^2/(4\pi\varepsilon_w k_B T) \approx 7$ Å, with the Boltzmann constant k_B and the ambient temperature $T = 300$ K.

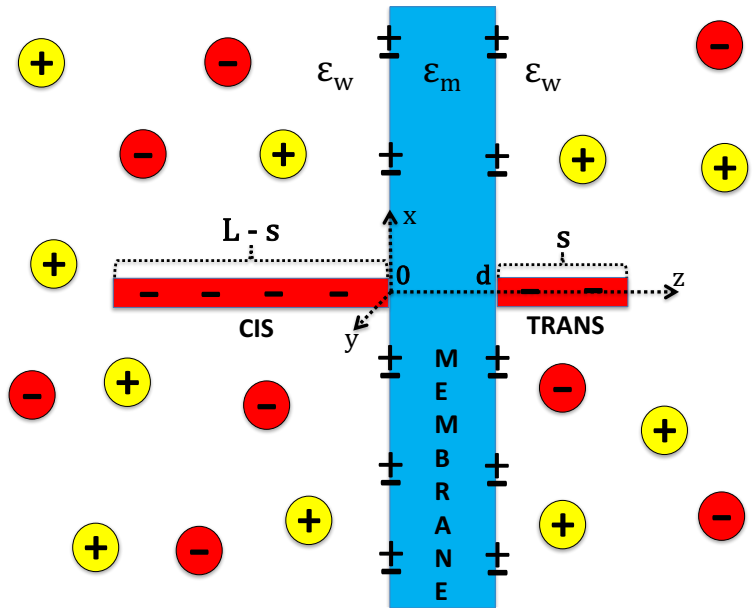


Figure 1. (color online) Schematic representation of the membrane of dielectric permittivity ε_m, thickness d, and negative or positive surface charge density σ_m. The membrane is immersed in the NaCl electrolyte with bulk density ρ_b and dielectric permittivity $\varepsilon_w = 80$. The polymer translocating through the pore has total length $L \gg d$. The length of the polymer portions on the *cis* to the *trans* sides is $L - s$ and s, respectively.

2.2. Modified Fokker–Planck Equation

The reaction coordinate of the translocation is the length s of the polymer portion on the *trans* side. The polymer portion on the *cis* side has length $L - s$ (see Figure 1). Thus, in our model, the contribution from the pore length to the translocation dynamics is neglected and the right end of the polymer penetrating the membrane is assumed to reach immediately the *trans* side. This is a reasonable approximation for the present case of thin membranes and long polymers $L \gg d$. This said, in the calculation of electrostatic polymer–membrane interactions, the finite thickness of the dielectric membrane will be fully taken into account.

The translocation dynamics is characterized by the Langevin equation

$$\gamma M \frac{\mathrm{d}s}{\mathrm{d}t} = -\eta_p \frac{\mathrm{d}s}{\mathrm{d}t} + f(s) + \xi(t), \tag{3}$$

where γ is the hydrodynamic friction coefficient. The first term on the r.h.s. of Equation (3) is the pore friction force and η_p the pore friction coefficient. The second term is the total external force $f(s) = -V_p'(s)$ acting on the polymer, with the polymer potential $V_p(s)$ including the effect of the externally applied electric force f_0 and electrostatic polymer–membrane interactions. Finally, the third term of Equation (3) corresponds to the Brownian force $\xi(t)$. In the bulk electrolyte, the diffusion coefficient of a cylindrical molecule is given by [24]

$$D_b = \frac{k_B T}{3\pi\eta L} \ln\left(\frac{2L}{ea}\right), \tag{4}$$

with the water viscosity $\eta = 8.91 \times 10^{-4}$ Pa s, Euler's number $e \approx 2.718$, and the DNA radius $a = 1$ nm. Thus, the corresponding hydrodynamic friction coefficient for the cylindrical molecule follows from Einstein's relation $MD_b\gamma = k_B T$ as

$$\gamma = \frac{3\pi\eta}{\lambda_m \ln(2L/ea)}, \tag{5}$$

where $\lambda_m = M/L$ is the linear polymer mass density.

In Appendix B, we show that the effective FP equation associated with the Langevin Equation (3) is given by

$$\partial_t c(s,t) = D_p \partial_s^2 c(s,t) + \beta D_p \partial_s \left[U_p'(s) c(s,t)\right], \tag{6}$$

where $c(s,t)$ is the polymer number density. In the dilute polymer regime where polymer–polymer interactions can be neglected, the function $c(s,t)$ also corresponds to the polymer probability density. In Equation (6), the effective pore diffusion coefficient is given by

$$D_p = \frac{\gamma k_B T}{M\gamma_p^2}, \tag{7}$$

with the net friction coefficient

$$\gamma_p = \gamma + \frac{\eta_p}{M}. \tag{8}$$

Finally, the effective polymer potential is

$$U_p(s) = \frac{\gamma_p}{\gamma} V_p(s). \tag{9}$$

2.3. Capture Velocity v_c and Translocation Time τ

We compute here the polymer translocation time τ corresponding to the time between the penetration of the polymer from the *cis* side and the exit of the molecule from the *trans* side, and the capture velocity v_c characterizing the penetration speed of the molecule into the pore. To this end, we express Equation (6) as an effective diffusion equation

$$\frac{\partial c(s,t)}{\partial t} = -\frac{\partial J(s,t)}{\partial s}, \tag{10}$$

with the polymer flux

$$J(s,t) = -D_p \partial_s c(s,t) - \beta D_p U_p'(s) c(s,t), \tag{11}$$

where the first and second terms on the r.h.s. correspond to the diffusive and convective flux components, respectively. We consider now the steady-state regime of the system characterized by a constant polymer flux $J(s,t) = J_{st}$ and density $c(s,t) = c_{st}(s)$. We recast Equation (11) in the form

$$J_{st} = -D_p e^{-\beta U_p(s)} \partial_s \left[c_{st}(s) e^{\beta U_p(s)}\right]. \tag{12}$$

Next, we integrate Equation (12) by imposing an absorbing boundary condition (BC) $c_{\rm st}(L) = 0$ at the pore exit. The absorbing BC assumes that, due to the deep voltage-induced electric potential on the *trans* side, the polymer that completes its translocation is removed from the system at $s = L$. One obtains

$$c_{\rm st}(s)e^{\beta U_{\rm p}(s)} = \frac{J_{\rm st}}{D_{\rm p}} \int_s^L {\rm d}s' e^{\beta U_{\rm p}(s')}. \tag{13}$$

Setting $s = 0$ in Equation (13), one gets the characteristic polymer capture velocity corresponding to the inward polymer flux per reservoir concentration $v_{\rm c} = J_{\rm st}/c_{\rm st}(0)$ as

$$v_{\rm c} = \frac{D_{\rm p}}{\int_0^L {\rm d}s\ e^{\beta\left[U_{\rm p}(s) - U_{\rm p}(0)\right]}}. \tag{14}$$

We note that Equation (14) corresponds to the characteristic speed at which the polymer reaches the minimum of the total electrostatic potential $V_p(z_p)$. In general, v_c differs from the average translocation velocity. The capture and translocation velocities coincide only in the specific case of drift-driven translocation considered in Section 3.1.

In order to derive the translocation time, we first note that the polymer population in the pore follows from the integral of Equation (13) in the form

$$N_{\rm p} = \int_0^L {\rm d}s\ c_{\rm st}(s) = \frac{J_{\rm st}}{D_{\rm p}} \int_0^L {\rm d}s\ e^{-\beta U_{\rm p}(s)} \int_s^L {\rm d}s'\ e^{\beta U_{\rm p}(s')}. \tag{15}$$

The translocation time corresponds to the inverse translocation rate. The latter is defined as the polymer flux per total polymer number, i.e., $\tau^{-1} = J_{\rm st}/N_{\rm p}$. This gives the polymer translocation time in the form

$$\tau = \frac{1}{D_{\rm p}} \int_0^L {\rm d}s e^{-\beta U_{\rm p}(s)} \int_s^L {\rm d}s' e^{\beta U_{\rm p}(s')}. \tag{16}$$

In Appendix C, we show that Equation (16) can be also derived from the Laplace transform of the FP Equation (6) as the mean first passage time of the polymer from $s = 0$ to $s = L$.

2.4. Electrostatic Polymer Potential $V_{\rm p}(s)$

The electrostatic potential experienced by the polymer reads

$$V_{\rm p}(s) = -f_0 s + \Delta\Omega_{\rm p}(s). \tag{17}$$

The first term on the r.h.s. of Equation (17) is the drift potential associated with the external force f_0. The second term including the polymer grand potential $\Delta\Omega_{\rm p}(s)$ accounts for electrostatic polymer–membrane interactions. In Appendix D, we show that this grand potential is given by

$$\Delta\Omega_{\rm p}(s) = \Omega_{\rm pm}(s) + \Delta\Omega_{\rm intra}(s) + \Delta\Omega_{\rm inter}(s). \tag{18}$$

The first term on the r.h.s. of Equation (18) corresponds to the direct interaction energy between the polymer and membrane charges,

$$\beta\Omega_{\rm pm}(s) = -\frac{2\tilde{\lambda}_{\rm c}}{\mu\kappa_{\rm b}^2}\left[2 - e^{-\kappa_{\rm b}(L-s)} - e^{-\kappa_{\rm b}s}\right] {\rm sign}(\sigma_{\rm m}), \tag{19}$$

with the Gouy–Chapman length $\mu = 1/(2\pi\ell_B|\sigma_m|)$ and DH screening parameter $\kappa_b = \sqrt{8\pi\ell_B\rho_b}$. Then, the second term of Equation (18) corresponding to the sum of the individual self interaction energies of the polymer portions on the *cis* and *trans* sides reads

$$\beta\Delta\Omega_{\text{intra}}(s) = \frac{\ell_B\tilde{\lambda}_c^2}{2}\int_0^\infty \frac{dkk}{p_b^3}\frac{\Delta\left(1-e^{-2kd}\right)}{1-\Delta^2e^{-2kd}}\left\{\left[1-e^{-p_bs}\right]^2+\left[1-e^{-p_b(L-s)}\right]^2\right\}, \tag{20}$$

where we defined the screening function $p_b = \sqrt{\kappa_b^2+k^2}$ and the dielectric jump function $\Delta = (\varepsilon_w p_b - \varepsilon_m k)/(\varepsilon_w p_b + \varepsilon_m k)$. Finally, the interaction energy between the trans and *cis* portions of the polymer is

$$\beta\Delta\Omega_{\text{inter}}(s) = \ell_B\tilde{\lambda}_c^2\int_0^\infty \frac{dkk}{p_b^3}\left\{\frac{\left(1-\Delta^2\right)e^{(p_b-k)d}}{1-\Delta^2e^{-2kd}}-1\right\}e^{-p_bd}\left[1-e^{-p_bs}\right]\left[1-e^{-p_b(L-s)}\right]. \tag{21}$$

3. Results and Discussion

3.1. Drift-Driven Regime

The drift-driven regime corresponds to the case of high salt density or strong external force f_0 where polymer membrane interactions can be neglected, i.e., $V_p(s) \approx -f_0 s$. In the drift limit, the effective polymer potential (9) takes the downhill linear form $\beta U_p(s) = -\lambda_0 s$ where we introduced the characteristic inverse length $\lambda_0 = \beta f_0\gamma_p/\gamma$. The capture velocity (14) and translocation time (16) become

$$v_c = \frac{D_p\lambda_0}{1-e^{-\lambda_0 L}}, \tag{22}$$

$$\tau = \frac{1}{D_p\lambda_0^2}\left[\lambda_0 L - 1 + e^{-\lambda_0 L}\right]. \tag{23}$$

For strong electric forces with $\beta f_0 L \gg 1$, Equations (22) and (23) take the standard drift form

$$v_c \approx v_{dr} = \frac{f_0}{\eta_p + \lambda_m\gamma L}, \tag{24}$$

$$\tau \approx \tau_{dr} = \frac{\eta_p L + \lambda_m\gamma L^2}{f_0}, \tag{25}$$

satisfying the drift-driven transport equation $\tau \approx L/v_c$. Considering that the logarithmic term in Equation (4) is of order unity, and introducing the characteristic length $L_c = \eta_p/(3\pi\eta)$, Equation (25) indicates that, for short polymers $L \ll L_c$, the translocation time exhibits a linear dependence on the polymer length, i.e., $\tau \approx (\eta_p/f_0)L$. For long polymers $L \gg L_c$, the translocation time grows quadratically with the polymer length as $\tau \approx (\lambda_m\gamma/f_0)L^2$. We note that these scaling laws also follow from the rigid polymer limit of the tension propagation theory [11].

We verified that the translocation dynamics is qualitatively affected by the pore friction only in the drift-driven regime considered above. Thus, in order to simplify the analysis of the model, from now on, we switch off the pore friction and set $\eta_p = 0$. This yields, in Equations (8) and (9), $\gamma_p = \gamma$. Consequently, the effective polymer potential in Equations (14) and (16) becomes $U_p(s) = V_p(s)$ or

$$U_p(s) = -f_0 s + \Omega_{pm}(s) + \Delta\Omega_{\text{intra}}(s) + \Delta\Omega_{\text{inter}}(s). \tag{26}$$

3.2. Neutral Membranes: Dielectric Trapping

We investigate here the electrostatics of polymer translocation through neutral membranes. In silicon nitride membranes, the neutral surface condition is reached by setting the acidity of the solution to the isoelectric point value pH ≈ 5 [25]. In this limit where $\sigma_m = 0$ and $\mu^{-1} = 0$, the polymer–membrane coupling energy in the polymer potential (26) vanishes, i.e., $\Omega_{pm}(s) = 0$.

3.2.1. Dielectric Trapping of the Polymer in Dilute Salt

To scrutinize the effect of polarization forces on the capture and translocation dynamics, we consider the simplest situation where the polymer is dressed by its counterions, but there is no additional salt in the solvent, i.e., $\rho_b = 0$. This corresponds to the limit $\kappa_b \to 0$ where the polymer self-energy components (20) and (21) become

$$\beta\Delta\Omega_{intra}(s) = \frac{\Delta_0}{2\ell_B}\int_0^\infty \frac{dk}{k^2}\frac{1-e^{-2kd}}{1-\Delta_0^2 e^{-2kd}}\left\{\left[1-e^{-ks}\right]^2+\left[1-e^{-k(L-s)}\right]^2\right\}, \quad (27)$$

$$\beta\Delta\Omega_{inter}(s) = -\frac{\Delta_0^2}{\ell_B}\int_0^\infty \frac{dk}{k^2}\frac{1-e^{-2kd}}{1-\Delta_0^2 e^{-2kd}}e^{-kd}\left[1-e^{-ks}\right]\left[1-e^{-k(L-s)}\right], \quad (28)$$

with the dielectric parameter $\Delta_0 = (\varepsilon_w - \varepsilon_m)/(\varepsilon_w + \varepsilon_m)$. According to Equations (26)–(28), in the limit of vanishing dielectric discontinuity $\varepsilon_m \to \varepsilon_w$ where $\Delta_0 = 0$, polymer–membrane interactions disappear and one recovers the drift behavior of Equations (24) and (25).

In Figure 2a,b, we display the polymer capture velocity v_c and translocation time τ against the dimensionless external force $\bar{f}_0 = \beta\ell_B f_0$ at various membrane permittivities $\varepsilon_m \leq \varepsilon_w$. One sees that, in the weak external force regime $\bar{f}_0 \lesssim 1$, polarization effects arising from the low membrane permittivity result in the deviation of v_c and τ from the linear response behavior of Equations (24) and (25). More precisely, the external force dependence of the translocation time switches from linear $\tau \sim f_0^{-1}$ for large forces $\bar{f}_0 \gtrsim 1$ to exponential $\ln\tau \sim -f_0$ for weak forces $\bar{f}_0 \lesssim 0.2$ (see also the inset of Figure 2b). The exponential decay of τ with f_0 is the sign of the barrier-driven translocation that we scrutinize below. Figure 2a,b also show that, at fixed force f_0, the dielectric discontinuity increases both the capture velocity v_c and the translocation time τ from their drift values, i.e., $\varepsilon_m \downarrow v_c \uparrow \tau \uparrow$. The mutual enhancement of v_c and τ is an important observation for nanopore-based sequencing techniques whose efficiency depends on fast polymer capture and extended ionic current signal.

The mechanism behind the enhanced capture speed and translocation time is illustrated in Figure 3a,b. The plots display the electrostatic self-energy profiles, and the renormalized polymer potential $U_p(s) - U_p(0)$ that includes the electric force f_0 and determines the capture velocity (14) and translocation time (16). First, we note that the self-energy component $\Delta\Omega_{intra}(s)$ is concave and repulsive (dotted curves in Figure 3a). Thus, the individual image–charge interactions of the *cis* and *trans* portions of the polymer act as an electrostatic barrier limiting the polymer capture by the pore. Then, one sees that the energy component $\Delta\Omega_{inter}(s)$ is convex and negative (dashed curves). Hence, the dielectric coupling between the *cis* and *trans* portions gives rise to an attractive force that favors the capture of the molecule.

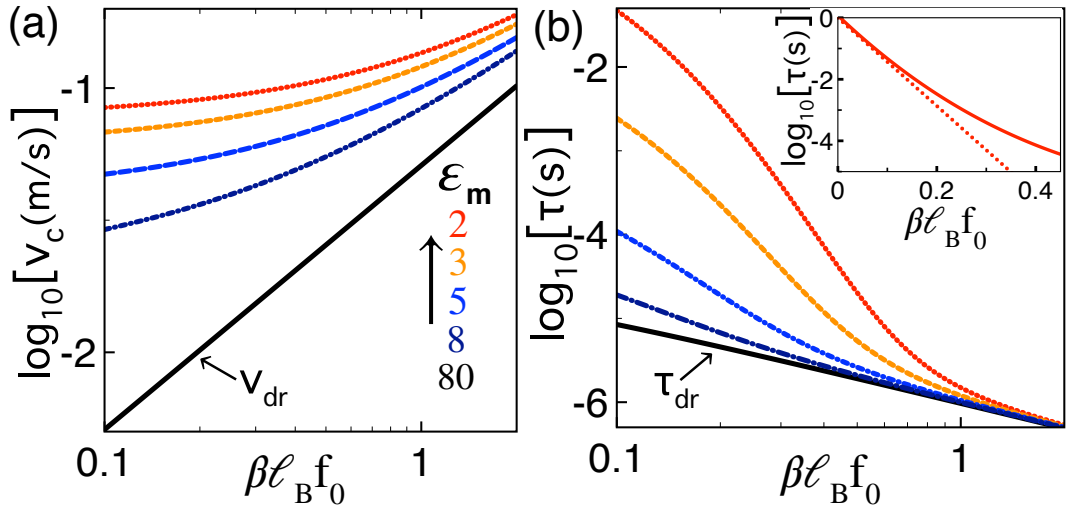


Figure 2. (color online) (**a**) polymer capture velocity (14) and (**b**) translocation time (16) versus the dimensionless external force $\bar{f}_0 = \beta \ell_B f_0$ in the dilute salt regime $\kappa_b = 0$ and at various membrane permittivity values ε_m given in the legend of (**a**). The black curve in (**b**) corresponds to the drift limit Equation (25) of the translocation time. The polymer length and membrane thickness are $L = 50$ nm and $d = 2$ nm. The pore friction is switched off, i.e., $\eta_p = 0$. The inset in (**b**) displays in a semilogarithmic plot the exponential regime of the translocation time for $\varepsilon_m = 2$.

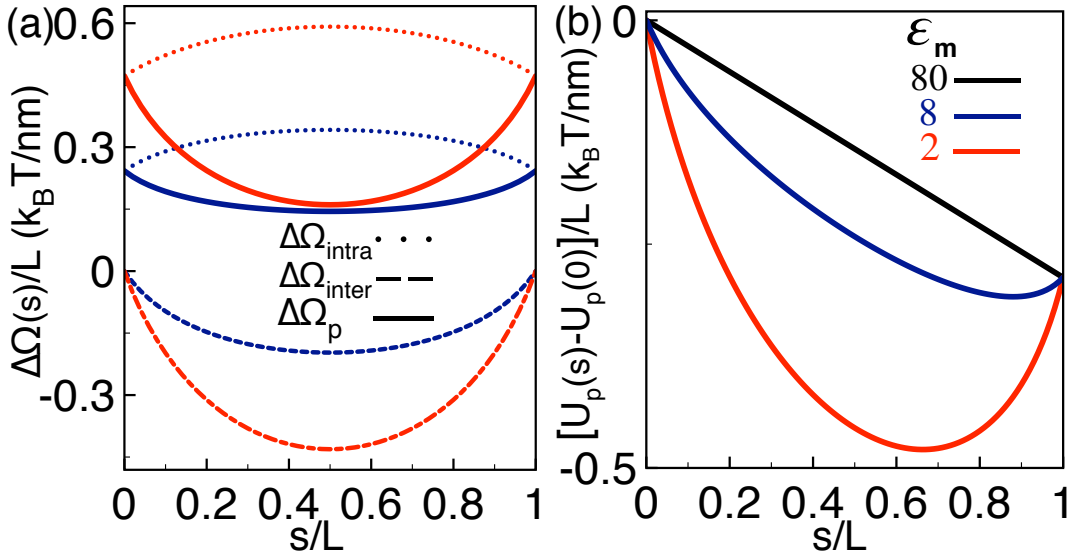


Figure 3. (color online) (**a**) profiles of the polymer self-energy components Equations (27) (dotted curves) and (28) (dashed curves), and the total self-energy in Equation (18) (solid curves); (**b**) effective polymer potential Equation (26) renormalized by its value at $s = 0$. In (**a**) and (**b**), the membrane permittivities are $\varepsilon_m = 80$ (black), 8 (navy), and 2 (red). The external force is $\bar{f}_0 = 0.2$. The other parameters are the same as in Figure 2.

In the present dilute salt conditions, the *trans-cis* coupling takes over the repulsive image–charge interactions. This gives rise to a purely convex and attractive total interaction potential $\Delta\Omega_p(s)$ whose slope is enhanced with the magnitude of the dielectric discontinuity, i.e., $\varepsilon_m \downarrow |\Delta\Omega_p'(s)| \uparrow$ (compare the solid curves in Figure 3a). Figure 3b shows that, as a result of this additional electrostatic force, the polymer potential develops an attractive well whose depth increases with the strength of the dielectric discontinuity, $\varepsilon_m \downarrow \ [U_p(s) - U_p(0)] \downarrow$. This dielectrically induced potential well speeds up the polymer capture but also traps the polymer at its minimum, resulting in the mutual enhancement of the polymer capture speed and translocation time in Figure 2a,b.

In order to localize the position of the dielectric trap, we pass to the asymptotic insulator limit $\varepsilon_m = 0$ where the grand potential components (27) and (28) can be evaluated analytically as $\beta\Delta\Omega_{intra}(s) = \ln(2)L/\ell_B$ and

$$\beta\Delta\Omega_{inter}(s) = -\frac{L}{\ell_B}\left\{\ln\left[\frac{L+d}{L+d-s}\right] + \frac{s}{L}\ln\left[\frac{L+d-s}{d+s}\right] + \frac{d}{L}\ln\left[\frac{d(d+L)}{(d+s)(d+L-s)}\right]\right\} \quad (29)$$

within this approximation, the solution of the equation $U_p'(s_*) = 0$ shows that the position of the trap rises linearly with the force f_0 and the polymer length L as

$$s_* \approx \frac{1}{2}\left[L + \left(d + \frac{L}{2}\right)\bar{f}_0\right]. \quad (30)$$

Equation (30) can be useful to adjust the location of the dielectric trap in translocation experiments.

3.2.2. Effect of Polymer Length and Finite Salt Concentration

We scrutinize here the alteration of the polymer translocation time and capture speed by the polymer length and salt concentration. Figure 4a shows that, at a given salt concentration, the length dependence of the translocation time is characterized by three regimes. At short polymer lengths $L < L_-$ where $L_- \approx 10$ nm corresponds to the upper boundary of the drift-driven translocation regime, polymer–membrane interactions and the self-energy $\Delta\Omega_p(s)$ are weak, and the translocation is characterized by drift transport, i.e., $\tau \approx \tau_{dr}$. Consequently, the translocation time of short polymers rises quadratically with the molecular length, i.e.,

$$\tau \propto L^2 \quad \text{for} \quad L < L_-. \quad (31)$$

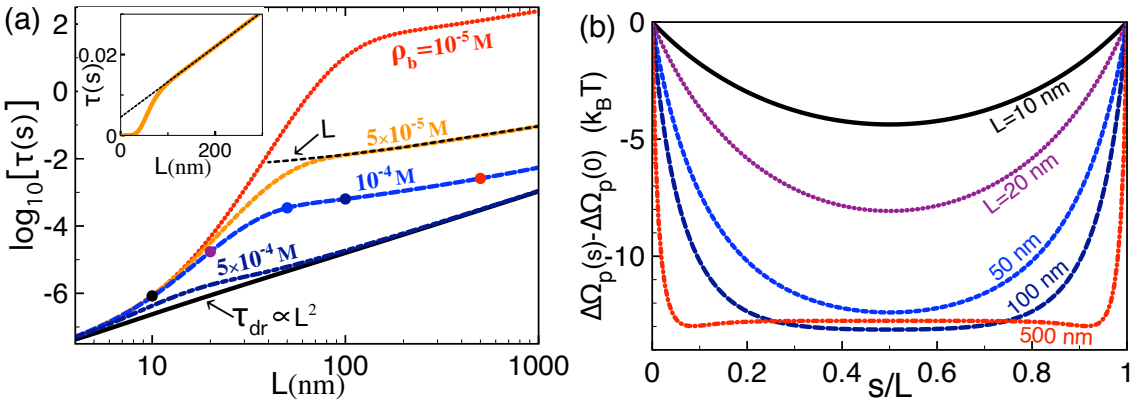


Figure 4. (color online) (**a**) translocation time of Equation (16) versus the polymer length at the membrane permittivity $\varepsilon_m = 2$ and various salt density values. The solid black curve corresponds to the drift limit Equation (25) of the translocation time. The inset displays the translocation time at $\rho_b = 5 \times 10^{-5}$ M in a linear scale; (**b**) renormalized polymer self-energy profile at the salt density $\rho_b = 10^{-4}$ M and various polymer lengths corresponding to the dots of the same color in (**a**). The external force and membrane thickness are $\bar{f}_0 = 0.2$ and $d = 2$ nm. In (**a**), the fast increase of the translocation time ends at the upper polymer length $L = L_+ = \kappa_b^{-1}$ with the numerical value $L_+ = 97$, 44, 31, and 20 nm, for $\rho_b = 10^{-5}$, 5×10^{-5}, 10^{-4}, and 5×10^{-4} M.

The departure from drift transport occurs at intermediate lengths $L > L_-$. In this regime, the magnitude of the attractive *trans-cis* coupling becomes significant and the increase of the polymer length strongly enhances the depth of the electrostatic potential trap (see Figure 4b). Figure 4a shows that this results in the amplification of the translocation time with the polymer length by orders of

magnitude. We found that this trend is the reminiscent of an exponential growth $\ln \tau \propto L$ reached in the asymptotic insulator limit $\varepsilon_{\mathrm{m}} = 0$ (data not shown).

The quick rise of the translocation time with the polymer length continues up to the characteristic length $L \approx L_+ = \kappa_{\mathrm{b}}^{-1}$ whose numerical value is given in the caption of Figure 4. L_+ corresponds to the critical polymer length beyond which electrostatic polymer–membrane interactions saturate. More precisely, due to salt screening, the *trans-cis* portions of the polymer separated by a distance larger than L_+ interact weakly. As a result, the depth of the dielectric trap is mostly invariant by the extension of the polymer length beyond L_+ (see Figure 4b). Thus, for $L \gtrsim L_+$, the value of the double integral in Equation (16) is not significantly affected by the length L, i.e., $\tau \propto D_{\mathrm{p}}^{-1} \propto L$. This results in the linear rise of the translocation time with the polymer length (see also the inset of Figure 4a), i.e.,

$$\tau \propto L \quad \text{for} \quad L > L_+. \tag{32}$$

We note that the scaling discussed above qualitatively agrees with experiments on α-Hemolysin pores exhibiting a similar piecewise length dependence of the translocation time (see, e.g., Figure 9 of Ref. [26]). Finally, Figure 4 shows that, due to the screening of dielectric polymer–membrane interactions, added salt reduces the translocation time, i.e., $\rho_{\mathrm{b}} \uparrow \tau \downarrow$. Beyond the characteristic salt concentration $\rho_{\mathrm{b}} \approx 10^{-4}$ M where the length L_+ approaches L_-, the translocation time tends to its drift limit at all polymer lengths.

3.3. Charged Membranes

We investigate here the alteration of the features discussed in Section 3.2 by a finite membrane charge. For a positive membrane charge $\sigma_m \geq 0$ corresponding to acidity values pH $\lesssim 5$ [25], the direct polymer–membrane coupling energy (19) results in an attractive force favoring the polymer capture. In order to characterize the effect of this additional force on the dielectric trapping mechanism, we first focus on the dilute salt regime and set $\rho_{\mathrm{b}} = 10^{-4}$ M. Figure 5a–c display the capture velocity, translocation time, and renormalized polymer potential at various weak membrane charge densities including the case of neutral membranes (navy curves).

One first notes that, upon the increase of the cationic membrane charge, the onset of the polymer–membrane attraction significantly deepens the trapping potential $U_p(s) - U_p(0)$. This enhances the translocation time of long polymers by orders of magnitude, i.e., $\sigma_{\mathrm{m}} \uparrow \tau \uparrow$ for $L \gtrsim 30$ nm. However, one also sees that, at the beginning of the translocation corresponding to the polymer capture regime $s \lesssim 0.2\ L$, the slope of the polymer potential is weakly affected by the increment of the membrane charge density. As a result, the dielectrically enhanced capture velocity v_c remains practically unaffected by a weak membrane charge. Finally, Figure 5b shows that the linear scaling of the translocation time with the polymer length remains unchanged by the surface charge, i.e., $\tau \propto L$ for $L \gtrsim L_+$ (see also the inset). One however notes that the finite membrane charge shifts the regime of linearly rising translocation time to larger polymer lengths, i.e., $\sigma_m \uparrow L_+ \uparrow$.

We consider now the stronger salt regime where the dielectric trapping effect disappears. To simplify the numerical computation of the capture velocity Equation (14) and translocation time Equation (16), we neglect the dielectric interaction terms of Equation (26) that become perturbatively small. Within this approximation, the polymer potential becomes $U_{\mathrm{p}}(s) \approx -f_0 s + \Omega_{\mathrm{pm}}(s)$.

Figure 6a–c show that, in the regime of moderate salt concentration and cationic membrane charge (purple and red curves), the direct polymer–membrane charge attraction can solely induce a deep enough electrostatic trap to enhance both the capture velocity and the translocation time by orders of magnitude, i.e., $\sigma_m \uparrow v_c \uparrow \tau \uparrow$. In terms of the dimensionless constant $c = \beta\mu\kappa_{\mathrm{b}} f_0/(4\tilde{\lambda}_{\mathrm{c}})$, the relation $U'_{\mathrm{p}}(s_*) = 0$ yields the location of the electrostatic trap in the form

$$\frac{s^*}{L} = 1 + \frac{1}{\kappa_{\mathrm{b}} L} \ln\left(c + \sqrt{c^2 + e^{-\kappa_{\mathrm{b}} L}}\right). \tag{33}$$

Equation (33) can enable to control the position of the polymer trap by changing the relative weight of the drift force f_0 and the electrostatic polymer–membrane attraction via the adjustment of various system parameters. Indeed, in the regime $\beta\mu\kappa_b f_0/(4\tilde{\lambda}_c) \ll 1$ corresponding to weak salt or external force f_0, and high membrane charge σ_m and/or polymer charge $\tilde{\lambda}_c$, Equation (33) indicates the trapping of the polymer at $s^* \approx L/2$. Moving to the opposite regime $\beta\mu\kappa_b f_0/(4\tilde{\lambda}_c) \gg 1$ of strong salt or external force, low membrane or polymer charge strength, and long polymers $\kappa_b L \gtrsim 1$, the trapping point in Equation (33) is shifted towards the polymer exit $s^* = L$ according to the relation

$$\frac{s^*}{L} \approx 1 - \frac{1}{\kappa_b L} \ln\left(\frac{2\tilde{\lambda}_c}{\beta\mu\kappa_b f_0}\right). \tag{34}$$

Figure 6b also shows that, at strong enough membrane charges (red curve), the trapping-induced enhancement of the translocation time is followed at large lengths by the linear scaling behavior $\tau \propto L$ equally observed for neutral and weakly charged membranes (see the inset of Figure 6c). At intermediate charges, the system tends to the drift behavior $\tau \to \tau_{dr}$ before the linear scaling regime is reached (purple curve in Figure 6b). We also note that, in the short length regime of Figure 6b, the weak curvature of the drift translocation time τ_{dr} stems from the logarithmic correction factor in the polymer diffusion coefficient of Equation (4).

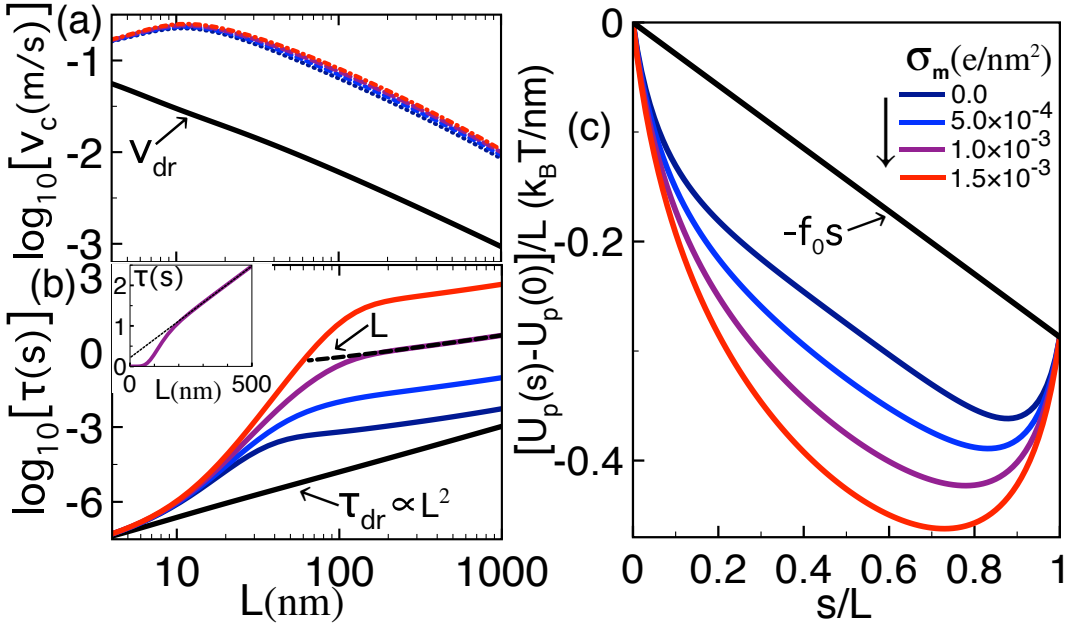


Figure 5. (color online) (**a**) polymer capture velocity Equation (14) and (**b**) translocation time Equation (16) against the polymer length L. The solid black curve in (**b**) corresponds to the drift limit Equation (25) of the translocation time; (**c**) effective polymer potential Equation (26) at $L = 100$ nm. The membrane charge density corresponding to each curve is given in the legend of (**c**). The inset in (**b**) displays the purple curve in a linear scale. Salt concentration is $\rho_b = 10^{-4}$ M. The other parameters are the same as in Figure 4.

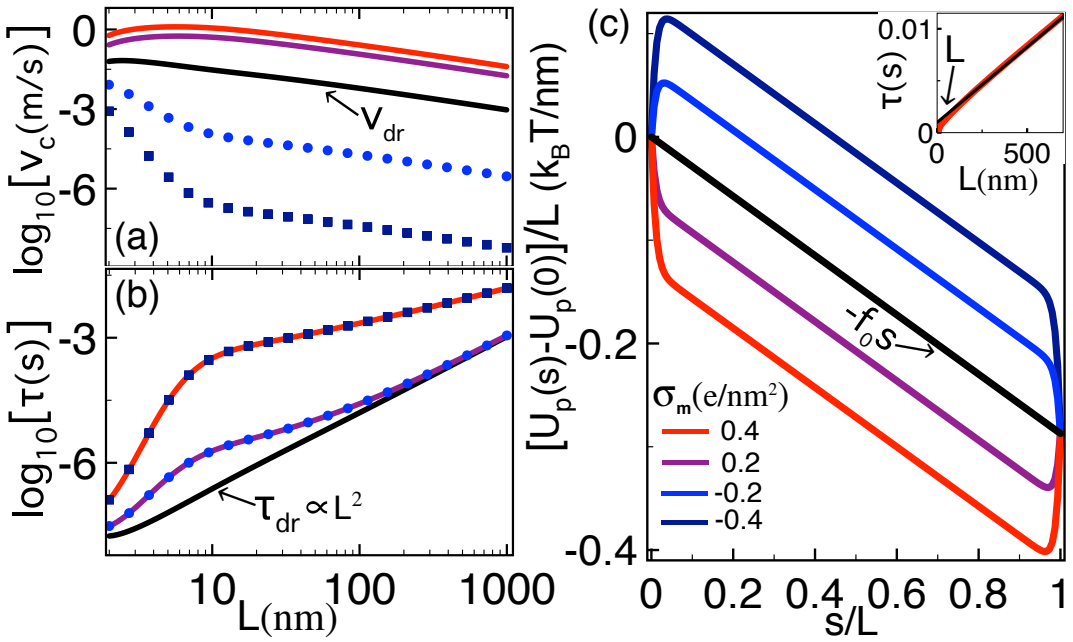


Figure 6. (Color online) (**a**) Polymer capture velocity Equation (14) and (**b**) translocation time Equation (16) against the polymer length L. The black curve in (**b**) corresponds to the drift limit Equation (25) of the translocation time. (**c**) Effective polymer potential (26) at $L = 100$ nm. The inset in (**c**) displays the red curve of (**b**) in a linear scale. The membrane charge density corresponding to each curve is given in the legend of (**c**). Salt concentration is $\rho_b = 0.1$ M. The other parameters are the same as in Figure 4.

We finally investigate the effect of anionic membrane charges reached in the acidity regime pH $\gtrsim 5$. Interestingly, Figure 6b indicates that, in strong salt conditions where the polymer–membrane charge coupling dominates the dielectrically induced polymer self-interactions, the enhancement of the translocation time in Equation (16) does not depend on the sign of the membrane charge, i.e., $\tau(\sigma_m) = \tau(-\sigma_m)$. However, one also notes that, in anionic membranes, the like-charge polymer–membrane repulsion gives rise to an electrostatic barrier at the pore entrance (see Figure 6c). Figure 6a shows that this barrier diminishes the polymer capture rate by several orders of magnitude, i.e., $|\sigma_m| \uparrow U_p(s) - U_p(0) \uparrow v_c \downarrow$ for $\sigma_m < 0$. Thus, in anionic membranes, the enhancement of the translocation time stems from the suppression of polymer capture by the electrostatic polymer–membrane repulsion. The existence of a similar barrier induced by electrostatic DNA-pore repulsion has been previously identified by a different polymer translocation model developed for long nanopores and short polymers [20].

4. Discussion

The accurate characterization of voltage-driven polymer translocation requires modeling of this process by including the electrostatic details of the polymer–membrane complex and the surrounding electrolyte solution. Motivated by this need, we have developed here an electrostatic transport model to investigate the effect of surface polarization forces, added salt, and membrane charge on the capture and translocation of stiff polymers with arbitrary length. Our results are summarized below.

We first considered the case of neutral membranes and dilute salt regime where the polyelectrolyte is dressed by its counterions, but there is no additional salt in the system. In this regime, we identified a dielectrically induced polymer trapping mechanism. Namely, the dielectric contrast between the low permittivity membrane and large permittivity solvent leads to attractive interactions between the *cis* and *trans* portions of the polymer. The attraction gives rise to a *dielectric trap* located at $s = s^* = [L + (d + L/2)\bar{f}_0]/2$. The trap speeds up the polymer capture occurring at $s < s^*$ but slows

down the escape of the polymer at $s > s^*$, amplifying the polymer capture velocity by several factors and the total translocation time by orders of magnitude.

We also observed that, in neutral membranes, added salt of concentration $\rho_b \gtrsim 10^{-4}$ M suppresses the dielectric trapping of the polymer. However, at arbitrary salt densities, positive membrane surface charges emerging at low solution pH restore the polymer trapping via the electrostatic polymer–membrane attraction. This *electrostatic trap* can enhance the polymer capture speed and translocation time as efficiently as its dielectric counterpart. It was also shown that the location of the trap in Equation (33) can be adjusted by modifying the experimentally accessible model parameters such as the salt and membrane charge density. Thus, the electrostatic trapping can equally well provide an efficient way to extend the duration of the ionic current blockade required for the sensitive sequencing of the translocating biopolymer.

Finally, we investigated the effect of polymer trapping on the scaling of the translocation time with the polymer length. At short lengths $L \lesssim 10$ nm where the interactions between the *cis* and *trans* sides of the polymer are dominated by the drift force f_0, the translocation is characterized by the drift behavior of Equation (25). In the intermediate polymer length regime 10 nm $\lesssim L \lesssim \kappa_b^{-1}$ where the attractive *trans-cis* coupling takes over the drift force, the resulting dielectric trap leads to a quasi-exponential inflation of the translocation time with the length of the molecule. Beyond the characteristic polymer length $L \approx \kappa_b^{-1}$ where ionic screening comes into play, the depth of the dielectric trap becomes saturated. As a result, the translocation time of long polymers rises linearly with the molecular length, i.e., $\tau \propto L$. We finally showed that, in positively charged membranes, the electrostatic trap results in a similar piecewise length dependence of the translocation time. It is also important to note that such a piecewise trend has been previously observed in translocation experiments with $\alpha-$Hemolysin pores [26].

The present formalism developed for long polymers and thin membranes is complementary to our previous translocation model of Ref. [20] introduced for short polymers translocating through long nanopores. These two formalisms can be unified in the future by taking into account both the detailed electrohydrodynamics of the nanopore and electrostatic polymer–membrane interactions outside the pore. This extension would also enable considering the influence of nonlinear electrostatic correlation effects such as polymer and pore charge inversion on the translocation dynamics [19].

Before concluding, we would like to comment about the stiff polymer approximation of the model. Considering the DNA persistence length $l_p \sim 50$ nm at the salt density $\rho_b = 0.1$ M, the entropic polymer fluctuations neglected in our model should become relevant for polymers of length $L \gtrsim 50$ nm. Thus, in the corresponding long polymer regime, the resulting entropic cost for polymer capture is expected to enhance the polymer translocation times and reduce the capture velocities from the predictions in Figure 6a,b. It should be, however, noted that as the remaining results reported in Figures 2–5 were obtained in the dilute electrolyte regime $\rho_b \leq 5 \times 10^{-4}$ M where DNA is stiffer than at the physiological salt density $\rho_b = 0.1$ M, our main conclusions should be qualitatively unaffected by the rigid rod approximation. A quantitatively accurate evaluation of the error caused by the stiff polymer approximation requires the direct inclusion of entropic polymer fluctuations into our model. This formidable task is beyond the scope of the present article. The consideration of this extension in a future work may also allow for incorporating into our electrostatic formalism the tension propagation mechanism relevant for long polymers [10,14].

Author Contributions: Conceptualization, S.B.; Investigation, S.B.; Writing—Original Draft Preparation, S.B., J.S. and T.A.N.; Visualization, S.B., J.S. and T.A.-N.; Funding Acquisition, T.A.-N.

Funding: This research was funded by the Academy of Finland QTF Centre of Excellence program (project 312298).

Conflicts of Interest: The authors declare no conflict of interest.

Appendix A. Variational Evaluation of the Dressed Polymer Charge

We summarize here the variational *charge renormalization* procedure that allows for evaluating the effective polymer charge density $\tilde{\lambda}_c$. The latter is defined as $\tilde{\lambda}_c = n\lambda_c$, where the charge renormalization factor n accounting for the counterion dressing of the bare charge λ_c follows from the numerical solution of the variational equation [23]

$$2(1-n)\ell_B\lambda_c\psi_p(a) + \kappa_b^2\int_a^\infty \mathrm{d}r r\left\{n\psi_p^2(r) - \psi_p(r)\sinh\left[n\psi_p(r)\right]\right\} = 0. \tag{A1}$$

In Equation (A1), the radius of the cylindrical polymer is $a = 1$ nm, and the electrostatic potential induced by the bare polymer charge reads

$$\psi_p(r) = \frac{2\ell_B\lambda_c}{\kappa_b a}\frac{K_0(\kappa_b r)}{K_1(\kappa_b a)}. \tag{A2}$$

In Equation (A2), we used the DH screening parameter $\kappa_b = \sqrt{8\pi\ell_B\rho_b}$ and the modified Bessel functions $K_n(x)$ [27]. We also note that, in the *Manning limit* of vanishing salt $\kappa_b \to 0$ where Equation (A1) yields $n = 1/(\ell_B\lambda_c)$, the net polymer charge becomes $\tilde{\lambda}_c = 1/\ell_B$.

Appendix B. Derivation of the FP Equation (6)

In this appendix, we derive the FP Equation (6) associated with the Langevin Equation (3). First, we cast this equation in the form

$$\gamma_p M\frac{\mathrm{d}s}{\mathrm{d}t} = f(s) + \xi(t), \tag{A3}$$

with the net friction coefficient

$$\gamma_p = \gamma + \frac{\eta_p}{M}, \tag{A4}$$

and the Gaussian white noise satisfying the relations

$$\langle\xi(t)\rangle = 0; \tag{A5}$$

$$\langle\xi(t)\xi(t')\rangle = 2M\gamma k_B T\delta(t-t'). \tag{A6}$$

In Equations (A5) and (A6), the bracket $\langle\cdot\rangle$ indicates the average over the Brownian noise. Integrating Equation (A3) over the infinitesimal time interval δt, one gets

$$\delta s(t) = \frac{1}{M\gamma_p}f(s)\delta t + \frac{1}{M\gamma_p}\int_t^{t+\delta t}\mathrm{d}t'\xi(t'). \tag{A7}$$

Taking the noise average of Equation (A7) and its square, and keeping only the terms linear in δt, one obtains

$$\langle\delta s(t)\rangle = \frac{1}{M\gamma_p}f(s)\delta t, \tag{A8}$$

$$\left\langle\delta s^2(t)\right\rangle = \frac{2\gamma k_B T\delta t}{M\gamma_p^2}. \tag{A9}$$

We now derive the stochastic equation generating the averages (A8) and (A9). Following the approach of Ref. [28], we start with the Chapman–Kolmogorov equation for the polymer translocation between the initial position $s_0 = s(t_0)$ and final position $s = s(t+\delta t)$,

$$c(s, t+\delta t; s_0, t_0) = \int_0^L \mathrm{d}s' c(s, t+\delta t; s', t)c(s', t; s_0, t_0). \tag{A10}$$

To progress further, we express the noise-averaged definition of the probability density

$$c(s, t + \delta t; s', t) = \left\langle \delta(s - s' - \delta s) \right\rangle, \tag{A11}$$

where the term δs on the r.h.s. corresponds to the random displacement over the infinitesimal time interval δt. Next, we Taylor-expand the corresponding term at order $O\left(\delta s^2\right)$ to obtain

$$c(s, t + \delta t; s', t) = \left\{ 1 + \langle \delta s \rangle \, \partial_{s'} + \frac{1}{2} \left\langle \delta s^2 \right\rangle \partial_{s'}^2 \right\} \delta(s - s'). \tag{A12}$$

Inserting Equation (A12) into Equation (A10), carrying out integrations by parts, and using the relations (A8) and (A9), one obtains

$$c(s, t + \delta t; s_0, t_0) = \left\{ 1 - \frac{\delta t}{M \gamma_\mathrm{p}} \partial_s f(s) + \delta t D_\mathrm{p} \partial_s^2 \right\} c(s, t; s_0, t_0), \tag{A13}$$

where we introduced the effective diffusion coefficient

$$D_\mathrm{p} = \frac{\gamma k_\mathrm{B} T}{M \gamma_\mathrm{p}^2}. \tag{A14}$$

Taylor-expanding the l.h.s. of Equation (A12), one gets

$$c(s, t + \delta t; s_0, t_0) = \{ 1 + \delta t \partial_t \} \, c(s, t; s_0, t_0). \tag{A15}$$

Equating the relations (A12) and (A15) and simplifying the result, one finally obtains the modified FP equation

$$\partial_t c(s, t) = D_\mathrm{p} \partial_s^2 c(s, t) + \beta D_\mathrm{p} \partial_s \left[U_\mathrm{p}'(s) c(s, t) \right] \tag{A16}$$

including the effective polymer potential

$$U_\mathrm{p}(s) = \frac{\gamma_\mathrm{p}}{\gamma} V_\mathrm{p}(s). \tag{A17}$$

Appendix C. Calculation of the Translocation Time

Here, based on the FP Equation (A16), we derive the polymer translocation time (15) as the mean first passage time of the polymer from the *cis* to the *trans* side. Our derivation will follow the approach of Ref. [29] that will be extended to the presence of a steady-state solution to the FP equation. The BCs associated with this equation are the initial condition at the pore mouth and an absorbing boundary at the pore exit,

$$c(s, t = 0) = \delta(s), \tag{A18}$$

$$c(s = L, t) = 0. \tag{A19}$$

The probability of polymer survival in the pore is

$$S(t) = \int_0^L \mathrm{d}s \; c(s, t). \tag{A20}$$

The translocation probability can be thus expressed as $P_\mathrm{tr}(t) = 1 - S(t)$ and the mean-first passage time distribution is therefore $\psi(t) = P_\mathrm{tr}'(t) = -S'(t)$, or

$$\psi(t) = -\int_0^L \mathrm{d}s \; \partial_t c(s, t). \tag{A21}$$

Thus, the translocation time corresponding to the mean-first passage time reads

$$\tau \equiv \int_0^\infty \mathrm{d}t\ \psi(t)t = -\int_0^L \mathrm{d}s \int_0^\infty \mathrm{d}t\ \partial_t c(s,t)t. \tag{A22}$$

We define now the transient part of the polymer density function

$$u(s,t) = c(s,t) - c_{\mathrm{st}}(s), \tag{A23}$$

with the steady-state polymer probability satisfying the equation $\partial_s^2 c_{\mathrm{st}}(s) + \beta\partial_s\left[U_{\mathrm{p}}'(s)c_{\mathrm{st}}(s)\right] = 0$. Thus, the transient solution (A23) equally satisfies the FP Equation (A16),

$$\partial_t u(s,t) = D_{\mathrm{p}}\partial_s^2 u(s,t) + \beta D_{\mathrm{p}}\partial_s\left[U_{\mathrm{p}}'(s)u(s,t)\right]. \tag{A24}$$

Next, we introduce the Laplace transform of Equation (A23),

$$Y(s,q) = \int_0^\infty \mathrm{d}t e^{-qt}u(s,t). \tag{A25}$$

After an integration by part, the translocation time (A22) becomes

$$\tau = \int_0^L \mathrm{d}s \int_0^\infty \mathrm{d}t\ u(s,t) = \int_0^L \mathrm{d}s\ Y_0(s), \tag{A26}$$

where we defined $Y_0(s) = Y(s, q = 0)$.

According to Equation (A24), given the initial condition (A18), the Laplace transform $Y_0(s)$ solves the differential equation

$$D_{\mathrm{p}}\partial_s^2 Y_0(s) + \beta D_{\mathrm{p}}\partial_s\left[U_{\mathrm{p}}'(s)Y_0(s)\right] = -\delta(s) - c_{\mathrm{st}}(s). \tag{A27}$$

Integrating Equation (A27) around the point $s = 0$ and taking into account the vanishing polymer probability for $z < 0$ outside the pore, one gets

$$Y_0'(0^+) + \beta U_{\mathrm{p}}'(0^+)Y_0(0^+) = -\frac{1}{D_{\mathrm{p}}}. \tag{A28}$$

Accounting now for the absorbing BC (A19), the homogeneous solution to Equation (A27) follows as

$$Y_0(s) = b\ e^{-\beta U_{\mathrm{p}}(s)}\frac{\int_s^L \mathrm{d}s' e^{\beta U_{\mathrm{p}}(s')}}{\int_0^L \mathrm{d}s' e^{\beta U_{\mathrm{p}}(s')}}, \tag{A29}$$

where b is an integration constant. Injecting the solution (A29) into Equation (A28), one finds $b = \int_0^L \mathrm{d}s' e^{\beta U_{\mathrm{p}}(s')}/D_{\mathrm{p}}$ and

$$Y_0(s) = \frac{1}{D_{\mathrm{p}}}e^{-\beta U_{\mathrm{p}}(s)}\int_s^L \mathrm{d}s' e^{\beta U_{\mathrm{p}}(s')}. \tag{A30}$$

Finally, the substitution of Equation (A30) into Equation (A26) yields the translocation time (15) of the main text.

Appendix D. Derivation of the Polymer Interaction Potential $\Delta\Omega_{\mathrm{p}}(s)$

In this appendix, we explain the calculation of the polymer–membrane interaction potential $\Delta\Omega_{\mathrm{p}}(s)$ in Equation (17) from the total polymer grand potential

$$\Omega_{\mathrm{p}}(s) = \Omega_{\mathrm{pm}}(s) + \Omega_{\mathrm{s}}(s). \tag{A31}$$

In Equation (A31), the term $\Omega_{\rm pm}(s)$ is the interaction energy between the polymer and membrane charges. The second component $\Omega_s(s)$ corresponds to the polymer self-energy accounting for the polarization forces induced by the dielectric contrast between the membrane and the solvent. Below, we review briefly the computation of these two potential components previously derived in Ref. [22]. The electrostatic potential $\Delta\Omega_{\rm p}(s)$ will be obtained from the grand potential (A31) at the end of Appendix D.2.

Appendix D.1. Polymer–Membrane Coupling Energy $\Omega_{\rm pm}(s)$

In Equation (A31), the grand potential component taking into account the polymer–membrane charge coupling is

$$\beta\Omega_{\rm pm}(s) = \int {\rm d}\mathbf{r}\sigma_{\rm p}(\mathbf{r})\phi_{\rm m}(\mathbf{r}), \tag{A32}$$

where we introduced the polymer charge density function

$$\sigma_{\rm p}(\mathbf{r}) = -\tilde{\lambda}_{\rm c}\delta(\mathbf{r}_{\parallel})\left[\theta(-z)\theta(z+l)+\theta(z-d)\theta(d+s-z)\right]. \tag{A33}$$

The first and second terms inside the bracket of Equation (A33) correspond to the *cis* and *trans* portions of the polymer with the respective lengths $l = L - s$ and s. Then, in Equation (A32), the average electrostatic potential $\phi_{\rm m}(\mathbf{r}) = \phi_{\rm m}(z)$ induced by the membrane charges satisfies the linear PB equation

$$\left[\partial_z\varepsilon(z)\partial_z - \kappa^2(z)\right]\phi_{\rm m}(z) = -4\pi\ell_{\rm B}\sigma_{\rm m}\left[\delta(z)+\delta(z-d)\right]. \tag{A34}$$

In Equation (A34), the dielectric permittivity and ionic screening functions read

$$\varepsilon(z) = \varepsilon_{\rm w}\left[\theta(-z)+\theta(z-d)\right]+\varepsilon_{\rm m}\theta(z)\theta(d-z), \tag{A35}$$

$$\kappa^2(z) = \kappa_{\rm b}^2\left[\theta(-z)+\theta(z-d)\right]. \tag{A36}$$

Solving Equation (A34) with the continuity condition $\phi_{\rm m}(z^-) = \phi_{\rm m}(z^+)$, and the jump condition $\varepsilon(z^+)\phi'(z^+) - \varepsilon(z^-)\phi'(z^-) = 4\pi\ell_{\rm B}\varepsilon_{\rm w}\sigma_{\rm m}$ at the charged boundaries located at $z = 0$ and $z = d$, one obtains

$$\phi_{\rm m}(z) = \frac{2}{\mu\kappa_{\rm b}}\left\{e^{\kappa_{\rm b}z}\theta(-z)+\theta(z)\theta(d-z)+e^{-\kappa_{\rm b}(z-d)}\theta(z-d)\right\}{\rm sign}(\sigma_m), \tag{A37}$$

with the Gouy–Chapman length $\mu = 1/(2\pi\ell_{\rm B}|\sigma_{\rm m}|)$. Substituting Equations (A33) and (A37) into Equation (A32), the polymer–membrane charge coupling potential finally becomes

$$\beta\Omega_{\rm pm}(s) = -\frac{2\tilde{\lambda}_{\rm c}}{\mu\kappa_{\rm b}^2}\left[1-e^{-\kappa_{\rm b}(L-s)}+1-e^{-\kappa_{\rm b}s}\right]{\rm sign}(\sigma_m). \tag{A38}$$

Appendix D.2. Polymer Self-Energy $\Delta\Omega_s(s)$ *and Total Electrostatic Polymer Potential* $\Delta\Omega_{\rm p}(s)$

The polymer self-energy component of Equation (A31) is given by

$$\beta\Omega_s(s) = \frac{1}{2}\int {\rm d}\mathbf{r}{\rm d}\mathbf{r}'\sigma_{\rm p}(\mathbf{r})v(\mathbf{r},\mathbf{r}')\sigma_{\rm p}(\mathbf{r}'), \tag{A39}$$

where the electrostatic kernel solves the DH equation

$$\left[\nabla\cdot\varepsilon(z)\nabla - \varepsilon(z)\kappa^2(z)\right]v(\mathbf{r},\mathbf{r}') = -\frac{e^2}{k_{\rm B}T}\delta(\mathbf{r}-\mathbf{r}'). \tag{A40}$$

Exploiting the planar symmetry and Fourier-expanding the kernel as

$$v(\mathbf{r},\mathbf{r}') = \int \frac{\mathrm{d}^2\mathbf{k}}{4\pi^2} e^{i\mathbf{k}\cdot(\mathbf{r}_\parallel - \mathbf{r}'_\parallel)} \tilde{v}(z,z'), \tag{A41}$$

the kernel Equation (A40) takes the one-dimensional form

$$\left[\partial_z \varepsilon(z)\partial_z - p^2(z)\right] \tilde{v}(z,z') = -\frac{e^2}{k_\mathrm{B}T}\delta(z-z'), \tag{A42}$$

where $p(z) = \sqrt{\kappa^2(z)+k^2}$. Defining now the bulk screening parameter $p_\mathrm{b} = \sqrt{\kappa_\mathrm{b}^2+k^2}$, the homogeneous solution of the linear differential Equation (A42) can be expressed as

$$\begin{aligned} \tilde{v}(z,z') &= b_1 e^{p_\mathrm{b} z}\theta(z'-z) + \left[b_2 e^{p_\mathrm{b} z} + b_3 e^{-p_\mathrm{b} z}\right]\theta(z-z')\theta(-z) \\ &+ \left[b_4 e^{kz} + b_5 e^{-kz}\right]\theta(z)\theta(d-z) + b_6 e^{-p_\mathrm{b} z}\theta(z-d), \end{aligned} \tag{A43}$$

for the charge source located at $z' < 0$, and

$$\begin{aligned} \tilde{v}(z,z') &= c_1 e^{p_\mathrm{b} z}\theta(z'-z) + \left[c_2 e^{p_\mathrm{b} z} + c_3 e^{-p_\mathrm{b} z}\right]\theta(z-z')\theta(-z) \\ &+ \left[c_4 e^{kz} + c_5 e^{-kz}\right]\theta(z)\theta(d-z) + c_6 e^{-p_\mathrm{b} z}\theta(z-d), \end{aligned} \tag{A44}$$

for $z' > 0$. In Equations (A43) and (A44), the coefficients b_i and c_i are integration constants. These constants are to be determined by imposing the continuity of the kernel $\tilde{v}(z,z')$ and the displacement field $\varepsilon(z)\partial_z\tilde{v}(z,z')$ at $z = 0$ and $z = d$, and by accounting for the additional relations $\tilde{v}(z'_-,z') = \tilde{v}(z'_+,z')$ and $\partial_z\tilde{v}(z,z')|_{z=z'+} - \partial_z\tilde{v}(z,z')|_{z=z'-} = -4\pi\ell_\mathrm{B}$ at the location of the source ion. After some long algebra, the Fourier-transformed kernel takes the form

$$\tilde{v}(z,z') = \tilde{v}_\mathrm{b}(z-z') + \delta\tilde{v}(z,z'). \tag{A45}$$

In Equation (A45), the first term is the Fourier transformed bulk DH kernel $\tilde{v}_\mathrm{b}(z-z') = (2\pi\ell_\mathrm{B}/p_\mathrm{b})e^{-p_\mathrm{b}|z-z'|}$. The second term corresponds to the dielectric part of the Green's function originating from the presence of the membrane. This dielectric component reads

$$\delta\tilde{v}(z,z') = \frac{2\pi\ell_\mathrm{B}}{p_\mathrm{b}} \frac{\Delta\left(1-e^{-2kd}\right)}{1-\Delta^2 e^{-2kd}} e^{p_\mathrm{b}(z+z')}, \tag{A46}$$

for $z \leq 0$ and $z' \leq 0$,

$$\delta\tilde{v}(z,z') = \frac{2\pi\ell_\mathrm{B}}{p_\mathrm{b}} \frac{\Delta\left(1-e^{-2kd}\right)}{1-\Delta^2 e^{-2kd}} e^{p_\mathrm{b}(2d-z-z')}, \tag{A47}$$

for $z \geq d$ and $z' \geq d$, and

$$\delta\tilde{v}(z,z') = \frac{2\pi\ell_\mathrm{B}}{p_\mathrm{b}} \frac{(1-\Delta^2)e^{(p_\mathrm{b}-k)d} + \Delta^2 e^{-2kd} - 1}{1-\Delta^2 e^{-2kd}} e^{-p_\mathrm{b}|z-z'|}, \tag{A48}$$

for $z' \leq 0$ and $z \geq d$, or $z' \geq d$ and $z \leq 0$. In Equations (A46)–(A48), we defined the dielectric jump function

$$\Delta = \frac{\varepsilon_\mathrm{w} p_\mathrm{b} - \varepsilon_\mathrm{m} k}{\varepsilon_\mathrm{w} p_\mathrm{b} + \varepsilon_\mathrm{m} k}. \tag{A49}$$

We finally note that, in Equations (A42)–(A49), the Fourier-transformed Green's function $\tilde{v}(z,z')$, the screening functions $p(z)$ and p_b, and the dielectric jump function Δ depend explicitly on the

two-dimensional wave vector k. In order to simplify the notation, the $k-$dependence of these functions will be omitted.

The net interaction potential $\Delta\Omega_{\rm p}(s)$ between the polymer and the charged dielectric membrane corresponds to the grand potential (A31) minus its bulk value. In the bulk reservoir where there is no charged interface, i.e., $\sigma_{\rm m}=0$, the polymer–membrane charge coupling energy (A38) naturally vanishes. Consequently, the interaction potential becomes

$$\Delta\Omega_{\rm p}(s)=\Omega_{\rm pm}(s)+\Delta\Omega_s(s), \tag{A50}$$

where the polymer self-energy renormalized by its bulk value is

$$\beta\Delta\Omega_s(s)=\frac{1}{2}\int \mathbf{dr}\mathbf{dr}'\sigma_{\rm p}(\mathbf{r})\left[v(\mathbf{r},\mathbf{r}')-v_{\rm b}(\mathbf{r}-\mathbf{r}')\right]\sigma_{\rm p}(\mathbf{r}'). \tag{A51}$$

Using Equations (A45)–(A48) in Equation (A51), after lengthy algebra, the self-energy Equation (A51) becomes

$$\Delta\Omega_s(s)=\Delta\Omega_{\rm intra}(s)+\Delta\Omega_{\rm inter}(s), \tag{A52}$$

with the individual self-energy of the polymer portions on the *cis* and *trans* sides of the membrane

$$\beta\Delta\Omega_{\rm intra}(s)=\frac{\ell_{\rm B}\tilde{\lambda}_{\rm c}^2}{2}\int_0^\infty\frac{{\rm d}kk}{p_{\rm b}^3}\frac{\Delta\left(1-e^{-2kd}\right)}{1-\Delta^2e^{-2kd}}\left\{\left[1-e^{-p_{\rm b}s}\right]^2+\left[1-e^{-p_{\rm b}(L-s)}\right]^2\right\}, \tag{A53}$$

and the energy of interaction between the *cis* and *trans* portions of the polymer

$$\beta\Delta\Omega_{\rm inter}(s)=\ell_{\rm B}\tilde{\lambda}_{\rm c}^2\int_0^\infty\frac{{\rm d}kk}{p_{\rm b}^3}\left\{\frac{\left(1-\Delta^2\right)e^{(p_{\rm b}-k)d}}{1-\Delta^2e^{-2kd}}-1\right\}e^{-p_{\rm b}d}\left[1-e^{-p_{\rm b}s}\right]\left[1-e^{-p_{\rm b}(L-s)}\right]. \tag{A54}$$

The net interaction potential (A50) can be finally expressed in terms of the energy components in Equations (A38), (A53) and (A54) as

$$\Delta\Omega_{\rm p}(s)=\Omega_{\rm pm}(s)+\Delta\Omega_{\rm intra}(s)+\Delta\Omega_{\rm inter}(s). \tag{A55}$$

References

1. Kasianowicz, J.J.; Brandin, E.; Branton, D.; Deamer, D.W. Characterization of individual polynucleotide molecules using a membrane channel. *Proc. Natl. Acad. Sci. USA* **1996**, *93*, 13770–13773. [CrossRef] [PubMed]
2. Henrickson, S.E.; Misakian, M.; Robertson, B.; Kasianowicz, J.J. Driven DNA transport into an asymmetric nanometer-scale pore. *Phys. Rev. Lett.* **2000**, *14*, 3057–3060. [CrossRef] [PubMed]
3. Meller, A.; Nivon, L.; Branton, D. Voltage-Driven DNA Translocations through a Nanopore. *Phys. Rev. Lett.* **2001**, *86*, 3435–3438. [CrossRef] [PubMed]
4. Bonthuis, D.J.; Zhang, J.; Hornblower, B.; Mathé, J.; Shklovskii, B.I.; Meller, A. Self-Energy-Limited Ion Transport in Subnanometer Channels. *Phys. Rev. Lett.* **2006**, *97*, 128104. [CrossRef] [PubMed]
5. Smeets, R.M.M.; Keyser, U.F.; Krapf, D.; Wue, M.-Y.; Dekker, N.H.; Dekker, C. Salt dependence of ion transport and DNA translocation through solid-state nanopores. *Nano Lett.* **2006**, *6*, 89–95. [CrossRef] [PubMed]
6. Clarke, J.; Wu, H.C.; Jayasinghe, L.; Patel, A.; Reid, S.; Bayley, H. Continuous base identification for single-molecule nanopore DNA sequencing. *Nat. Nanotechnol.* **2009**, *4*, 265–270. [CrossRef] [PubMed]
7. Wanunu, M.; Morrison, W.; Rabin, Y.; Grosberg, A.Y.; Meller, A. Electrostatic focusing of unlabelled DNA into nanoscale pores using a salt gradient. *Nat. Nanotechnol.* **2010**, *5*, 160–165. [CrossRef] [PubMed]
8. Sung, W.; Park, P.J. Polymer Translocation through a Pore in a Membrane. *Phys. Rev. Lett.* **1996**, *77*, 783. [CrossRef] [PubMed]
9. Luo, K.; Huopaniemi, I.; Ala-Nissila, T.; Ying, S.C. Polymer translocation through a nanopore under an applied external field. *J. Chem. Phys.* **2006**, *124*, 114704. [CrossRef] [PubMed]

10. Sakaue, T. Nonequilibrium dynamics of polymer translocation and straightening. *Phys. Rev. E* **2007**, *76*, 021803. [CrossRef] [PubMed]
11. Ikonen, T.; Bhattacharya, A.; Ala-Nissila, T.; Sung, W. Unifying model of driven polymer translocation. *Phys. Rev. E* **2012**, *85*, 051803. [CrossRef] [PubMed]
12. Farahpour, F.; Maleknejad, A.; Varnikc, F.; Ejtehadi, M.R. Chain deformation in translocation phenomena. *Soft Matter* **2013**, *9*, 2750–2759. [CrossRef]
13. Palyulin, V.V.; Ala-Nissila, T.; Metzler, R. Polymer translocation: The first two decades and the recent diversification. *Soft Matter* **2014**, *10*, 9016–9037. [CrossRef] [PubMed]
14. Sarabadani, J.; Ala-Nissila, T. Theory of pore-driven and end-pulled polymer translocation dynamics through a nanopore: An overview. *J. Phys. Condens. Matter* **2018**, *30*, 274002. [CrossRef] [PubMed]
15. Ghosal, S. Effect of Salt Concentration on the Electrophoretic Speed of a Polyelectrolyte through a Nanopore. *Phys. Rev. Lett.* **2007**, *98*, 238104. [CrossRef] [PubMed]
16. Zhang, J.; Shklovskii, B.I. Effective charge and free energy of DNA inside an ion channel. *Phys. Rev. E* **2007**, *75*, 021906. [CrossRef] [PubMed]
17. Wong, C.T.A.; Muhtukumar, M. Polymer translocation through alpha-hemolysin pore with tunable polymer-pore electrostatic interaction. *J. Chem. Phys.* **2010**, *133*, 045101. [CrossRef] [PubMed]
18. Grosberg, A.Y.; Rabin, Y. DNA capture into a nanopore: Interplay of diffusion and electrohydrodynamics. *J. Chem. Phys.* **2010**, *133*, 165102. [CrossRef] [PubMed]
19. Buyukdagli, S.; Ala-Nissila, T.; Blossey, R. Ionic current inversion in pressure-driven polymer translocation through nanopores. *Phys. Rev. Lett.* **2015**, *114*, 088303. [CrossRef] [PubMed]
20. Buyukdagli, S.; Ala-Nissila, T. Controlling Polymer Capture and Translocation by Electrostatic Polymer-pore interactions. *J. Chem. Phys.* **2017**, *147*, 114904. [CrossRef] [PubMed]
21. Buyukdagli, S. Facilitated polymer capture by charge inverted electroosmotic flow in voltage-driven polymer translocation. *Soft Matter* **2018**, *14*, 3541–3549. [CrossRef] [PubMed]
22. Buyukdagli, S.; Ala-Nissila, T. Electrostatics of polymer translocation events in electrolyte solutions. *J. Chem. Phys.* **2016**, *145*, 014902. [CrossRef] [PubMed]
23. Netz, R.R.; Orland, H. Variational charge renormalization in charged systems. *Eur. Phys. J. E Soft Matter* **2003**, *11*, 301–311. [CrossRef] [PubMed]
24. Avalos, J.B.; Rubi, J.M.; Bedeaux, D. Dynamics of rodlike polymers in dilute solution. *Macromolecules* **1993**, *26*, 2550–2561. [CrossRef]
25. Firnkes, M.; Pedone, D.; Knezevic, J.; Döblinger, M.; Rant, U. Electrically facilitated translocations of proteins through silicon nitride nanopores: Conjoint and competitive action of diffusion, electrophoresis, and electroosmosis. *Nano Lett.* **2010**, *10*, 2162–2167. [CrossRef] [PubMed]
26. Meller, A.; Branton, D. Single molecule measurements of DNA transport through a nanopore. *Electrophoresis* **2002**, *23*, 2583–2591. [CrossRef]
27. Abramowitz, M.; Stegun, I.A. *Handbook of Mathematical Functions*; Dover Publications: New York, NY, USA, 1972.
28. Siegman, A.E. Simplified derivation of the Fokker-Planck equation. *Am. J. Phys.* **1979**, *47*, 545–547. [CrossRef]
29. Ansalone, M.; Chinappi, L.; Rondoni, L.; Cecconi, F. Driven diffusion against electrostatic or effective energy barrier across α-hemolysin. *J. Chem. Phys.* **2015** *143*, 154109. [CrossRef]



© 2018 by the authors. Licensee MDPI, Basel, Switzerland. This article is an open access article distributed under the terms and conditions of the Creative Commons Attribution (CC BY) license (http://creativecommons.org/licenses/by/4.0/).